PAPER

Check for updates

Synthesis and photocatalytic properties of three dimensional laminated structure anatase TiO₂/nano-Fe⁰ with exposed (001) facets

Yeshuo Dong [ID] *[a] and Fanjun Meng[b]

Three dimensional laminated structure anatase TiO_2/nano-Fe^0 with exposed (001) facets used as photocatalysts were synthesized by a two-step solvothermal route and a liquid phase reduction deposition method. The resulting samples were characterized by X-ray diffraction, X-ray photoelectron spectroscopy, ultraviolet-visible diffuse reflectance spectroscopy, scanning electron microscopy, transmission electron microscopy and selected-area electron diffraction. Characterization and experimental results indicated that the three dimensional laminated structure of anatase TiO_2 was assembled by two dimensional TiO_2-sheets with a thickness of approximately 30 nm. The three dimensional laminated structure anatase TiO_2/nano-Fe^0 photocatalysts with improved visible-light responsive capability, high charge-hole mobility, and low electron–hole recombination exhibited higher photocatalytic performance in the photocatalytic degradation of methylene blue. The composite of nano-Fe^0 and TiO_2 could effectively promote the generation of hydroxyl radicals (˙OH) with a synergistic effect and Photo-Fenton theory. This study provided new insights into the fabrication and practical application of high-performance photocatalysts in degrading organic pollutants.

1. Introduction

The increasingly serious problems of energy shortages and environmental pollution have become a critical obstacle to the sustainable development of society.[1,2] The photocatalysis technology based on inorganic semiconductor catalysis materials provides us with an ideal new way of energy utilization and environmental pollution control.[3–5] Many inorganic semiconductor materials have been widely studied and applied in the field of environmental protection, dye-sensitized solar cells, photoelectric conversion and water decomposition hydrogen production due to their unique structural characteristics and excellent physical and chemical properties.[6–8] As we all know, in many inorganic semiconductor materials, TiO_2 has been deeply studied for a long time due to its simple processing, stable chemical properties and being harmless to the environment and humans.[9,10] Because of these excellent characteristics, it is usually used in the treatment of organic wastewater (such as dyes). Compared with the anodic oxidation,[11] electrocoagulation,[12] adsorption,[13,14] and biodegradation methods,[15] it has the advantages of strong oxidation, low energy consumption and simple operation. However, nano-TiO_2 grains have the defects of low

visible light utilization, easy recombination of photogenerated electrons and holes, and easy agglomeration and deactivation at nano scale.[16,17] The studies show that for a long time, the research on the design and preparation of TiO_2 semiconductor materials is the key to improve the comprehensive performance of photocatalysis.[18,19] It is the core scientific problem in the field of TiO_2 semiconductor photocatalysis that the materials have high efficiency of excitation light response, excellent electron hole yield and separation characteristics.[20–22] Therefore, scholars have carried out a series of research on the reconstruction of self structure and auxiliary modification based on the design and preparation of TiO_2 morphology and structure.[16,17,23,24]

In recent years, it has been shown that with the development of crystal surface engineering, it is popular to adjust the performance of photocatalytic materials by adjusting the exposure degree of crystal surface in the study of TiO_2 structure reconstruction.[25,26] In 2008, the uniform anatase TiO_2 single crystals were synthesized with a large percentage (47%) of reactive (001) facets using hydrofluoric acid as a morphology controlling agent.[27] This material shows a higher photocatalytic activity than that of conventional TiO_2 with (101) facets. Subsequently, the research of anatase TiO_2 single crystal with (001) facets has attracted great attention, and on this basis, TiO_2 nanosheets with higher (001) facets exposure ratio have been synthesized.[28–30] When the proportion of anatase TiO_2 with exposed (001) facets increased, the photocatalytic activity of TiO_2 improved significantly.

[a]School of Environmental and Municipal Engineering, Qingdao University of Technology, Qingdao, 266033, China. E-mail: dysh_1127@aliyun.com

[b]College of Chemistry, Chemical Engineering and Materials Science, Shandong Normal University, Jinan, 250014, China

However, TiO_2 nanosheets usually have the defects of easy agglomeration, easy lose electron and poor dispersion.[25] Therefore, researchers have used different titanium sources and improved synthesis methods to realize the self-assembly of TiO_2 single crystal sheets with (001) facets exposed, and some TiO_2 catalysts with multi-level structure such as spherical and flower structure formed by the self-assembly of TiO_2 single crystal sheets with (001) facets have been successively synthesized.[31–33] The self-assembly structure of the single crystal sheets can effectively improve the transmission efficiency of photogenerated electrons and promote the separation of photogenerated electrons and holes, thus greatly improving the photocatalytic activity and photoelectric effect.[34,35] Therefore, the research on the design and preparation of TiO_2 materials with (001) facets exposed sheets structure has great significance and broad application prospects.[21,36,37]

In the study of TiO_2 assisted modification, the addition of transition and/or noble metals is one of the promising methods to improve the photocatalytic activity and photoelectric effect of TiO_2.[38–41] Due to the formation of doping energy and the rapid transfer of the photogenerated electrons from the semiconductors to the dopants, the doped metal such as Fe, Pt, Mo, Cr, Ag and Au can reduce the recombination rate of electrons and holes.[42] As a new environmental remediation engineering material, nano-zerovalent iron (nano-Fe^0) has been widely used in the field of environmental remediation. Nano-Fe^0 has the excellent properties of large specific surface area, high chemical reaction activity and excellent surface characteristics, which make it suitable for the treatment of many pollutants that are difficult to biodegrade.[43–45] Up to now, nano-Fe^0 has been proved to be able to effectively remove a variety of pollutants, including nitroaromatic compounds, organic halogenated compounds, inorganic nitrates, polycyclic aromatic hydrocarbons, organic dyes, a variety of heavy metals and antibiotic drugs.[46,47] However, the high activity of nano-Fe^0 makes its stability in the air very poor, and it is easy to be oxidized or even self-ignited after contacting with oxygen.[48,49] Because of its nano size, it is easy to agglomerate in the water, which limits the application of nano-Fe^0 materials in the actual water treatment process.[50,51] Many results show that the combination of nano-Fe^0 and TiO_2 can effectively improve the stability of nano-Fe^0 and the dispersion in the water.[52] At the same time, this combination can effectively promote the separation of photogenerated electron holes, enhance the photoelectric effect, and expand the visible light response range. Moreover, in the process of photocatalysis, this combination can not only compensate the consumption of nano-Fe^0 (dynamic circulation reaction mechanism),[53] but also form the Photo-Fenton effect; Fe^{3+}; Fe^{2+}; TiO_2 and H_2O_2 coexisting in the system will promote the production of hydroxyl radicals under the action of ultraviolet light, so as to improve the photocatalytic activity and pollutant removal rate.[52,54,55]

In this work, we aim to synthesize a highly active composite TiO_2 photocatalyst with (001) facets exposed and visible light response by combining nano-Fe^0. Therefore, under the action of hydrofluoric acid, isobutanol and isopropanol, three dimensional laminated structure anatase TiO_2/nano-Fe^0 with exposed (001) facets (3D-TiO_2/nano-Fe^0) were synthesized by a two-step solvothermal route and a liquid phase reduction deposition method. The structure and morphology of samples were characterized by X-ray diffraction (XRD), scanning electron microscopy (SEM), transmission electron microscope (TEM), X-ray photoelectron spectroscopy (XPS) and UV-vis diffuse reflectance spectra (UV-vis DRS), respectively. Besides, methylene blue was used as the degradation substrate. The synergistic effect and photocatalytic properties of 3D-TiO_2/nano-Fe^0 photocatalysts on methylene blue were investigated by adjusting the pH value, the concentration of dissolved oxygen and the band of excitation light.

2. Experimental methods

2.1 Synthesis of 3D laminated structure anatase TiO_2 with exposed (001) facets

The 3D laminated structure anatase TiO_2 with exposed (001) facets (3D-TiO_2) were synthesized in a two-step solvothermal route (Scheme 1). In this work, hydrofluoric acid (HF), isobutanol and isopropanol were used as the morphology controlling agent.[56] We synthesized these 3D-TiO_2 by controlling the interaction characteristics of hydrofluoric acid (HF), isobutanol and isopropanol on the crystal facets.

Firstly, titanium tetrafluoride (TiF_4; Sigma-Aldrich) was dissolved in hydrochloric acid solution under vigorous stirring to give a concentration of 0.04 mol L^{-1} with the pH value changed to 2.60 mL of the above TiF_4 solution (0.04 mol L^{-1}) and 10 mL of isobutanol were added into a 100 mL Teflon-lined stainless steel autoclave. The autoclave was kept at 180 °C for 6 h in an electric oven. After reaction, the white solid TiO_2 particles were harvested by centrifugation, cleaning and drying.

Secondly, the obtained white solid TiO_2 particles were used as seeds. 10 mL of isobutanol, 20 mL of isopropanol and 0.1 mL of hydrofluoric acid (HF, 40 wt%) were added into a 50 mL Teflon-lined stainless steel auto-clave. The autoclave was kept at 200 °C for 15 h in an electric oven. After centrifugation, washing and drying, the 3D-TiO_2 were harvested. The surface fluorine was removed at 500 °C for 90 min. Then, the samples were cooled to room temperature for further activity experiments and characterization.
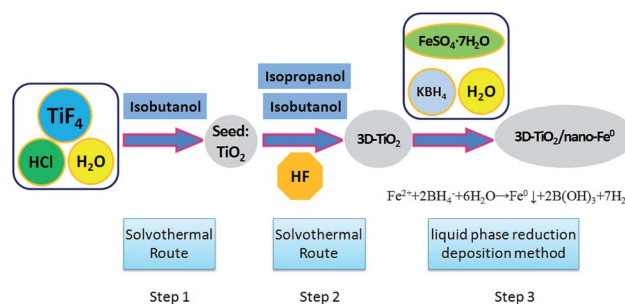
Scheme 1 Synthesis route of 3D laminated structure anatase TiO_2/nano-Fe^0 photocatalysts (3D-TiO_2/nano-Fe^0).

2.2 Synthesis of 3D laminated structure anatase TiO₂/nano-Fe⁰ photocatalysts

The 3D laminated structure anatase TiO_2/nano-Fe⁰ photocatalysts (3D-TiO_2/nano-Fe⁰) were synthesized by a liquid phase reduction deposition method (Scheme 1). In a typical process, the prepared 3D laminated structure anatase TiO_2 samples (0.8 g), C_2H_5OH (50 mL) and $FeSO_4 \cdot 7H_2O$ solution (0.6 mol L^{-1}; 100 mL) were mixed, stirred and ultrasonic dispersion 30 min under nitrogen protection. And then the mixture was centrifuged and dried to get the solid particles M. Then, M (1.0 g) and C_2H_5OH (60 mL) were mixed and stirred constantly for 30 min to get the component X. Alkaline KBH_4 solution (pH = 9; 0.4 mol L^{-1}) was dropped in X under stirring, and the reaction mixture was treated by ultrasonic intermittently until the black solid suspension was obtained. After precipitation, filter, cleaning, rotary steam drying. Finally, the 3D-TiO_2/nano-Fe⁰ photocatalysts were obtained and stored in the anaerobic environment.

2.3 Characterization of materials

The morphology and structure of the as-synthesized 3D-TiO_2/nano-Fe⁰ photocatalysts were investigated by X-ray spectroscopy (XRD, Bruker D8 Advance), scanning electron microscopy (SEM, JEOL-JSM6400F), UV-vis diffuse reflectance spectra (UV-vis DRS, Lambda 35) and transmission electron microscopy (TEM, JEM-2100) equipped with a selected-area electron diffraction (SAED). X-ray photoelectron spectroscopy (XPS) measurements were conducted by a Kratos AXIS Ultra DLD XPS system.

2.4 Photocatalytic properties measurement

Methylene blue (thiazine dye), an environment pollutant, was selected to evaluate the photocatalytic activities of 3D-TiO_2/nano-Fe⁰ photocatalysts under UV and visible light irradiation. The experiments were conducted using an airtight reactor. High-purity nitrogen and oxygen were purged continuously to maintain anoxic and oxic conditions. A 350W UV-light lamp was positioned within the central part of the photoreactor and cooling water was circulated through a pyrex jacket surrounding the lamp. The reactants were taken from the suspension at regular time intervals and immediately filtered through a 0.22 μm polytetrafluoroethylene filter membrane, and the filtrate was collected for analysis. An UV-vis absorption spectrophotometer (UV-2500, Shimadzu) was used to determine the absorbance of products.

3. Results and discussion

3.1 Characterization

In this work, the structure of samples have been confirmed by X-ray diffraction (XRD), and the diffraction pattern are shown in Fig. 1. Anatase TiO_2 was observed in the samples, which indicated that its crystallinity was not affected by the nano-Fe⁰. The diffraction patterns of the prepared anatase TiO_2 correlated well with the standard peaks (JCPDS card no. 21-1272), with the three most obvious diffraction peaks observed at 25.5° (101), 37.9° (004), and 48.2° (200). The (004) diffraction peak can be
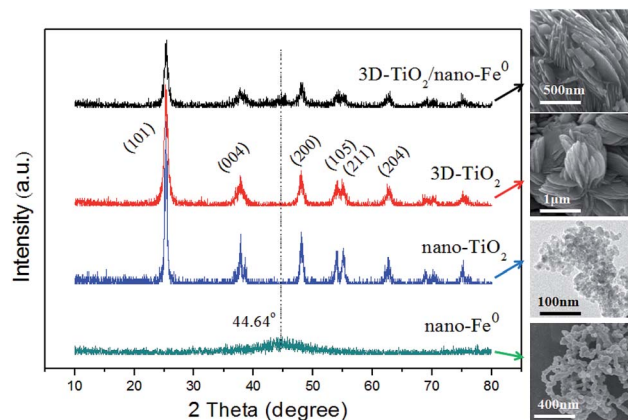

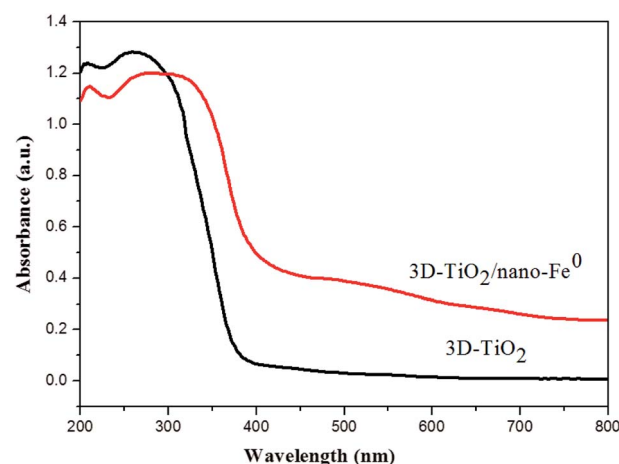Fig. 1 XRD patterns of nano-Fe⁰; nano-TiO_2; 3D-TiO_2 and 3D-TiO_2/nano-Fe⁰.

Fig. 2 UV-vis DRS of the 3D-TiO_2 and 3D-TiO_2/nano-Fe⁰ photocatalyst.

identified in the XRD pattern, which indicated the TiO_2 nanostructures along the (001) crystallographic direction.[28,57] In the curve of both the nano-Fe⁰ and 3D-TiO_2/nano-Fe⁰, the characteristic peak at the 2θ of 44.64° belonged to α-Fe (110) crystal was observed, suggesting that in the 3D-TiO_2/nano-Fe⁰ composite the nano-Fe⁰ keeps its original properties.[53] The crystallite sizes of the 3D-TiO_2/nano-Fe⁰, 3D-TiO_2, nano-Fe⁰ and nano-TiO_2 were obtained by both SEM images analysis (Fig. 3 and 4) and Scherrer formula calculation, obtaining average values of 3.5 μm, 3 μm, 80 nm and 10 nm, respectively.

Considering that band structure plays a key role in determining the photocatalytic activity of semiconductors, the UV-vis DRS of the synthesized samples were performed. As shown in Fig. 2, a significant increase was found in the visible absorption of 3D-TiO_2/nano-Fe⁰ photocatalysts compared with 3D-TiO_2. Concerning to the band gap energy (E_g) values, there was a visible-shift in the absorption edge for 3D-TiO_2/nano-Fe⁰ photocatalysts compared to the 3D-TiO_2. Moreover, compared with the optical absorption of 3D-TiO_2 cut off at 385 nm, it can be seen that the absorption peak of the 3D-TiO_2/nano-Fe⁰
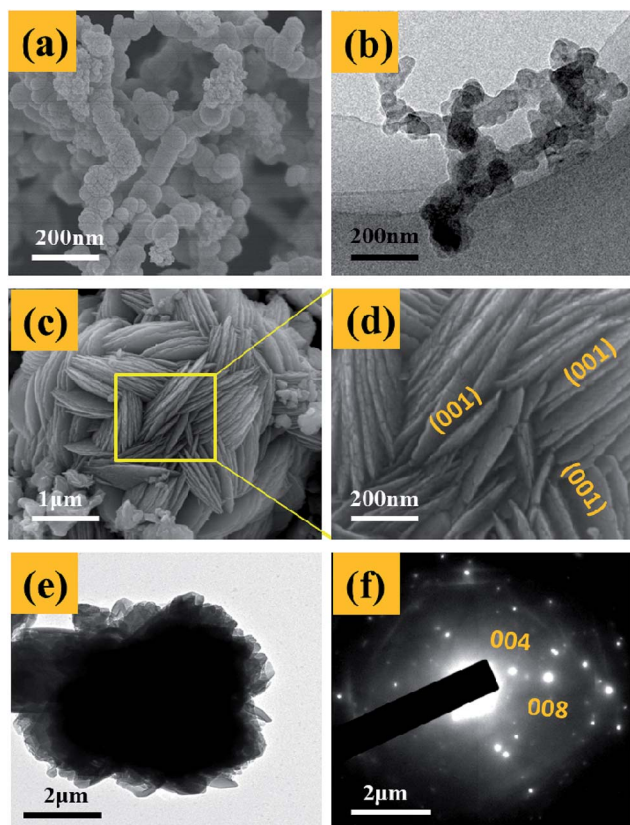
Fig. 3 Microstructure and morphology of samples. (a) and (b), SEM and TEM images of typical nano-Fe[0] particles. (c) and (d), SEM images of typical 3D-TiO_2. (e), TEM images of 3D-TiO_2. The corresponding selected-area electron diffraction (SAED) patterns was shown in (f).

photocatalysts in the visible region was stronger than that of the 3D-TiO_2. It indicates that the prepared 3D-TiO_2/nano-Fe[0] photocatalysts showed a photoresponse red shift effect by reducing the band gap energy of TiO_2, which is consistent with the photocatalytic activity shown in Fig. 8

Fig. 3 presents the SEM and TEM images of the nano-Fe[0] (Fig. 3a and b) and 3D-TiO_2 (Fig. 3c–e). As shown in Fig. 3a and b, the morphology of nano-Fe[0] is ball chain-shaped with a size of approximately 50 nm, which generally has agglomeration phenomenon. SEM images in Fig. 3c and d showed the general morphology of the 3D-TiO_2, which were entirely composed of 3D laminated structures with a size of approximately 3 μm. The 3D laminated structures were assembled by 2D TiO_2-sheets with a thickness of approximately 30 nm. The microstructures of the 3D-TiO_2 were investigated by TEM and selected-area electron diffraction (SAED). TEM image showed the 3D laminated structures in which 3D-TiO_2 can be easily identified in Fig. 3e. And the corresponding SAED patterns shown in Fig. 3f indicated that the top and bottom facets of the TiO_2 nanosheets were the (001) facets.[31] Fig. 4 presents the SEM (a and b) and TEM (c and d) images of the 3D-TiO_2/nano-Fe[0]. According to SEM, we can see clearly that there are many nano-Fe[0] particles on the surface of 3D-TiO_2. Moreover, the high-resolution TEM image recorded in Fig. 4d clearly shows the atomic planes with the lattice spacing of 0.204 nm and 0.19 nm, which corresponding to the (110) planes of α-Fe and the (200) planes of TiO_2, respectively. This result proved the formation of heterojunctions between nano-Fe[0] and TiO_2. And the formed heterojunction structure can not only block the recombination of the photogenerated electron–hole effectively, but also reduce the band gap energy of TiO_2. Thus, the 3D-TiO_2/nano-Fe[0] photocatalysts show a high response and high catalytic activity in the
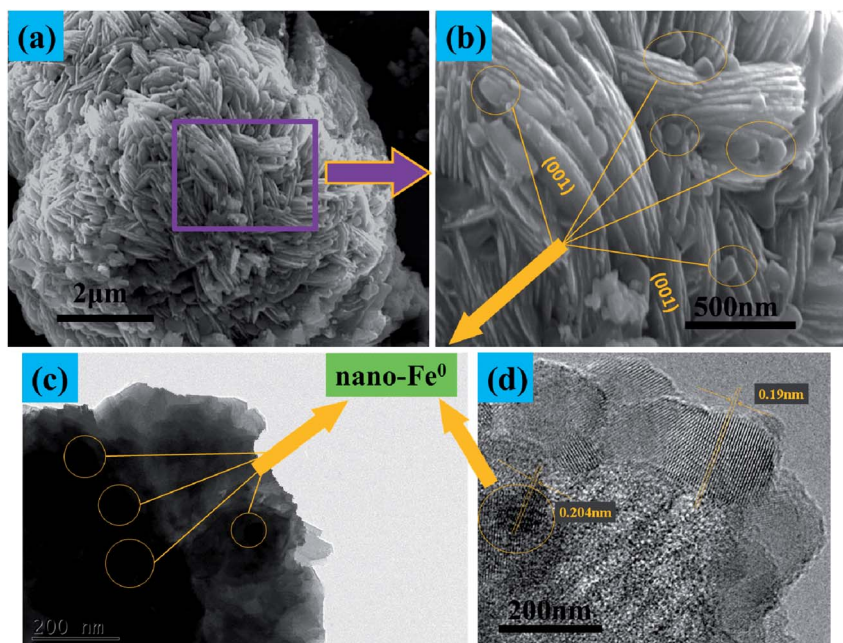

Fig. 4 (a) and (b), SEM images of typical 3D-TiO_2/nano-Fe[0] photocatalysts. (c) and (d), TEM and HRTEM images of 3D-TiO_2/nano-Fe[0] photocatalysts.

visible region, which is consistent with the analysis results of the UV-vis DRS shown in Fig. 2.

As shown in Fig. 5, XPS was used to determine the surface chemical compositions and chemical states of the resultant crystals. It can be seen that 3D-TiO_2/nano-Fe^0 contain Ti, O, and C elements, with sharp photoelectron peaks appearing at binding energies of 458 eV, 531 eV and 285 eV, respectively.[58] The C 1s (285 eV) peak is attributed to the adventitious hydrocarbon from XPS instrument itself. Fig. 5 (inset) is the XPS of the nano-Fe^0 in the 2p region. The photoelectron peaks appearing at binding energies of 711 eV, 719.9 eV and 724.5 eV represent the $2p_{3/2}$ peak, the vibrational satellite peak of $2p_{3/2}$ and $2p_{1/2}$ peak, respectively. The binding energy values of Fe element show that there are iron oxides on the surface of nano-Fe^0. Besides, there is a small photoelectron peak at 707 eV, which represent the $2p_{3/2}$ peak of nano-Fe^0. The analysis shows that the surface of nano-Fe^0 is covered by iron oxides.

3.2 Photocatalytic performance

Methylene blue (thiazine dye) is an aromatic heterocyclic compound, which has important applications in chemical indicators, pharmaceutical production, dyes (pigments) preparation and other fields.[14,59] However, dye wastewater is characterized by complex composition, high chroma, large discharge and poor biodegradability, and mostly contains carcinogenic, teratogenic and mutagenic substances.[2,60] Traditional wastewater treatment technology is weak in mineralization of refractory organics, so it can not be completely transformed into harmless small molecules.[61] Due to the limitations of traditional water treatment technology, aiming at the scientific problem of degradation and removal of methylene blue, the related experiments were carried out in this paper. Therefore, based on the characteristics and mechanism of photocatalytic oxidation of TiO_2, the degradation of methylene blue by TiO_2 photocatalysis technology was studied in this work.
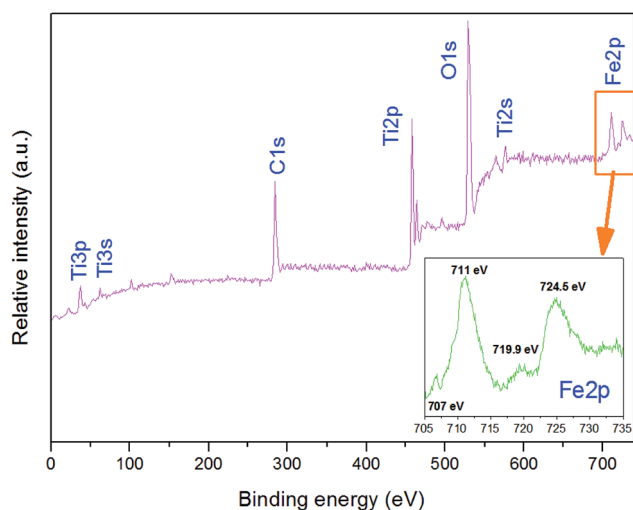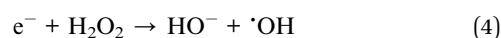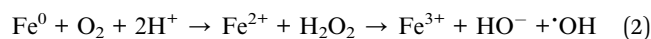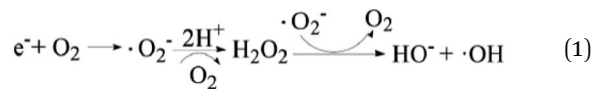

Fig. 5 XPS survey spectra of the as-synthesized 3D-TiO_2/nano-Fe^0 photocatalysts.

As shown in Fig. 6, the effect of the initial pH value on the degradation efficiency with different samples are investigated. It can be seen that the initial pH value of the dye aqueous solution affects the degradation efficiency obviously for both 3D-TiO_2 and 3D-TiO_2/nano-Fe^0, and an acidic pH value is benefit for a high degradation efficiency.[62] The reason for this is that the H^+ was a very key reaction factor to promote the generation of hydroxyl radicals (˙OH). According to the mechanism of the photocatalytic oxidation reaction, the isoelectric point of TiO_2 is pH_{PZC} = 6.8. In the acidic range (pH < pH_{PZC}), the surface of catalyst is protonated and results in a positive charge surface, which can promote the photo-generated electron transfer to the catalyst surface.[63] The comparison of dark reaction experiments showed that the 3D-TiO_2/nano-Fe^0 photocatalyst had higher degradation activity in the dark reaction. This is because in the absence of light conditions, nano-Fe^0 can play a priority role in the degradation of dyes. Moreover, the presence of iron ions in an acidic environment can cause flocculation, which will also increase the degradation efficiency.[64]

As shown in Fig. 6a, for the 3D-TiO_2/nano-Fe^0 photocatalyst, the degradation activity is low when it is in alkaline conditions. When the pH > 7, ferrous hydroxide ($Fe(OH)_2$) was obtained due to the reaction of zerovalent iron with water produced Fe^{2+} and OH^-. $Fe(OH)_2$ would further transform to ferric oxides under alkaline conditions. That will destroy the balance of the reaction and accelerate nano-Fe^0 consumption. Moreover, the ferric oxides will deposit onto the surface of catalysts to prevent contact with contamination. Therefore, the removal and degradation of pollutants is not conducive by the 3D-TiO_2/nano-Fe^0 photocatalyst in the alkaline environment.

The effect of dissolved oxygen on the degradation efficiency of methylene blue was investigated, and the results were shown in Fig. 7. It can be seen that the degradation efficiency will be higher in oxic condition for both 3D-TiO_2 and 3D-TiO_2/nano-Fe^0. According to the principle of heterogeneous photocatalysis (eqn (1)), the dissolved oxygen can act as a reactant and an photo-electron capture agent. The dissolved oxygen will combine with photoelectron and proton to produce H_2O_2. Then H_2O_2 reacts with superoxide anion radical (˙O^{2-}) to produce hydroxyl radical (˙OH).

$$e^- + O_2 \longrightarrow \cdot O_2^- \xrightarrow[O_2]{2H^+} H_2O_2 \xrightarrow{\overset{\cdot O_2^-}{} \overset{O_2}{}} HO^- + \cdot OH \tag{1}$$

$$Fe^0 + O_2 + 2H^+ \rightarrow Fe^{2+} + H_2O_2 \rightarrow Fe^{3+} + HO^- + \cdot OH \tag{2}$$

$$H_2O_2 \xrightarrow{h\nu} 2\cdot OH \tag{3}$$

$$e^- + H_2O_2 \rightarrow HO^- + \cdot OH \tag{4}$$

For the 3D-TiO_2/nano-Fe^0 photocatalyst, the nano-Fe^0 will reacts with dissolved oxygen and H^+ to produce H_2O_2 (eqn (2)). This degradation step takes place *via* oxidizing agents such as H_2O_2 and other oxidative species in oxic condition which in turn
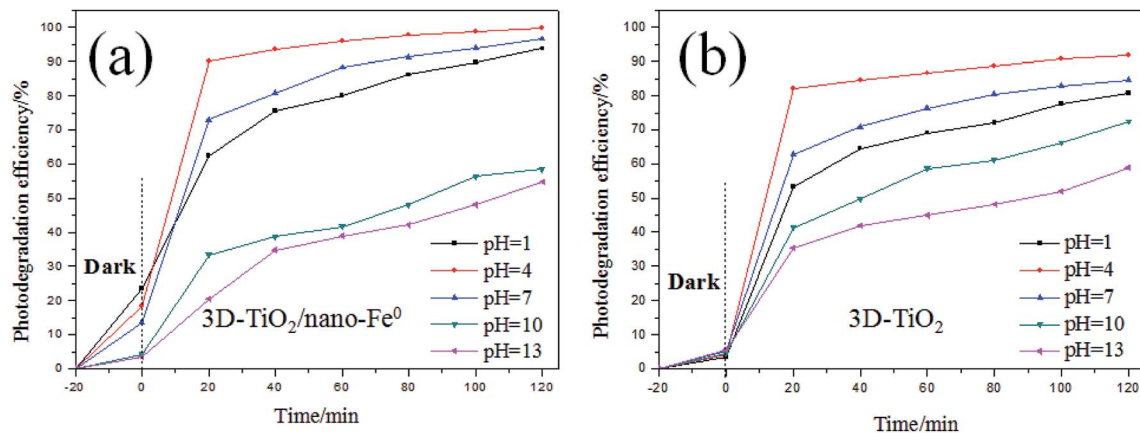
Fig. 6 Comparion on photocatalytic degradation activity of samples under different pH. (a) 3D-TiO$_2$/nano-Fe^0; (b) 3D-TiO$_2$.
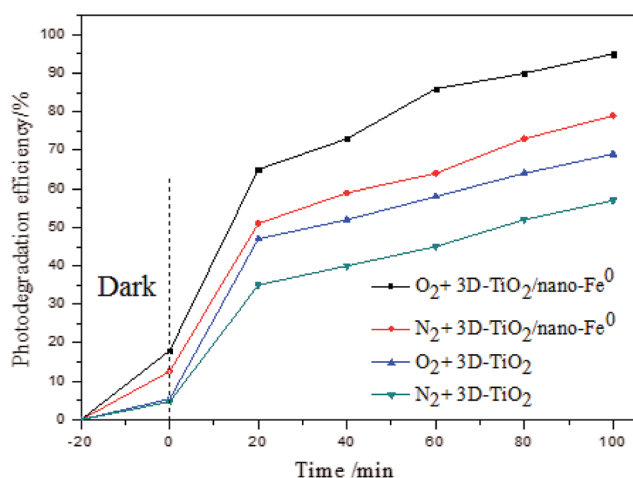

Fig. 7 Comparion on photocatalytic degradation activity of samples under the different concentration of dissolved oxygen.

produce hydroxyl radical through Fenton process (eqn (2)). Moreover, under the condition of photocatalysis, one part of H$_2$O$_2$ will be photolyzed into hydroxyl radical (eqn (3)), and the other part will react with photoelectrons to produce hydroxyl radical (eqn (4)). So, the 3D-TiO$_2$/nano-Fe^0 photocatalyst shows higher catalytic activity than the 3D-TiO$_2$, which further proves that the nano-Fe^0 will promote the photocatalytic activity by Photo-Fenton theory. Beside, in view of synergistic effect, the TiO$_2$ photocatalysts can be photoexcited by UV light to generate electron–hole pairs. The nano-Fe^0 on the surface of 3D-TiO$_2$ can accelerate the charge transfer and separation, leading to the enhancement of the oxidation. In addition, the produced Fe^{2+} in reaction system can react with photogenerated holes to form Fe^{3+}, and then be converted back to Fe^{2+} again when reacted with electrons, resulting in the prevention of hole–electron recombination and the increase in the total amounts of hydroxyl radicals.[64]

The degradation efficiency of methylene blue with different catalyst and light source are tested and compared, and the results are shown in Fig. 8. It is obvious that the catalytic activity of 3D-TiO$_2$/nano-Fe^0 photocatalysts was higher than 3D-TiO$_2$ under both UV and visible light. As shown in Fig. 2, the 3D-TiO$_2$/nano-Fe^0 shows a high absorbance in the visible region, thus the 3D-TiO$_2$/nano-Fe^0 will respond to visible light and produces photocatalytic activity. This result is mainly due to the formation of heterojunction structure, which is consistent with the analysis results of the UV-vis DRS shown in Fig. 2.

As we all know, in the research of photocatalytic degradation of dyes, the decolorization rate is usually used as the index of photocatalytic degradation activity.[65–67] However, the fading of dye only means that its chromophore is destroyed, rather than it is completely mineralized into H$_2$O and CO$_2$. In order to evaluate the degradation efficiency of photocatalysis strictly, we studied the relationship between the decolorization rate and COD$_{Cr}$ removal rate. As shown in Fig. 9a, the decolorization rate is not equivalent to the COD$_{Cr}$ removal rate. When the decolorization rate reaches 100%, the COD$_{Cr}$ removal rate is 55%, which demonstrates that when the chromophore of dye is destroyed under the system of photocatalysis, it will lead to fading effect. After photocatalytic degradation, some
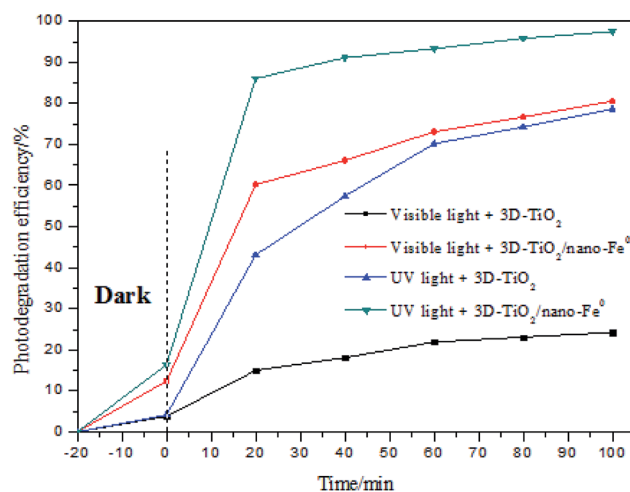

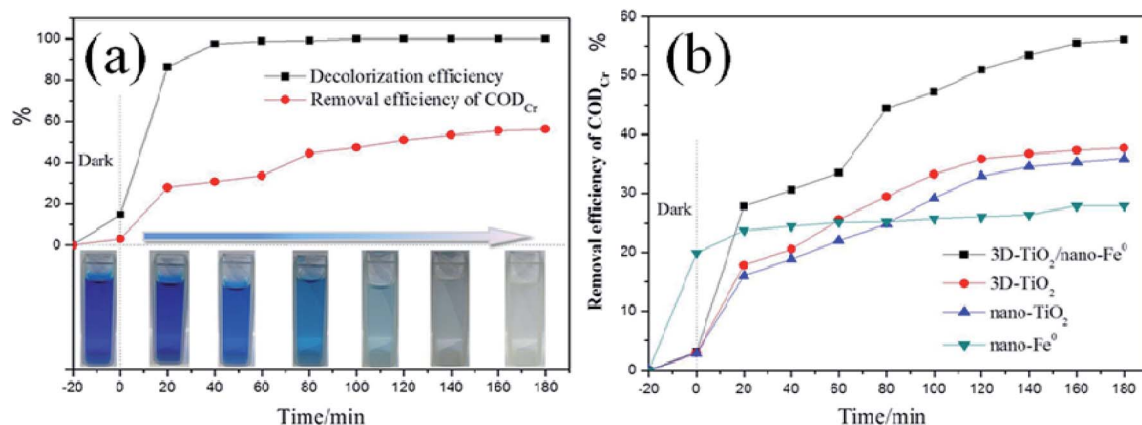Fig. 8 Comparion on photocatalytic degradation activity of samples under UV light and under visible light.

Fig. 9 (a), Comparison of decolorization rate and COD_{Cr} in photocatalytic process. (b), COD_{Cr} removal rate under the different samples.

intermediates that are difficult to be photocatalytic degraded will still exist in the system. Moreover, the removal efficiency of different samples for COD_{Cr} was tested showing that the 3D-TiO_2/nano-Fe^0 photocatalysts has a higher removal efficiency for the COD_{Cr} due to its synergistic effect and Photo-Fenton theory (Fig. 9b).

Although it has higher accuracy to evaluate the photocatalytic efficiency with the COD_{Cr}, it is more complex. In this case, considering the trend consistency of decolorization rate and COD_{Cr} removal rate and the fast determination of decolorization rate, the decolorization rate is used as the measurement index, which is scientific and feasible.

4. Conclusions

In summary, the 3D-TiO_2/nano-Fe^0 photocatalysts could be synthesized by a two-step solvothermal route and a liquid phase reduction deposition method. The characterization results confirmed that the 3D-TiO_2/nano-Fe^0 photocatalysts had three dimensional laminated structure which assembled by two dimensional TiO_2-sheets with a thickness of approximately 30 nm. Moreover, the composite of nano-Fe^0 leaded to the visible light response characteristics of the catalyst. On the application side, the resultant 3D-TiO_2/nano-Fe^0 photocatalysts exhibited remarkable photocatalytic performance for the degradation of methylene blue, which could be largely attributed to their synergistic effect and Photo-Fenton theory. Most significantly, the 3D-TiO_2/nano-Fe^0 photocatalysts has a higher removal efficiency for the COD_{Cr}, which provides a new material and approach for the mineralization of organic pollutants.

Conflicts of interest

There are no conflicts to declare.

References

1 Z. F. Huang, J. J. Zou, L. Pan, S. B. Wang, X. W. Zhang and L. Wang, *Appl. Catal., B*, 2014, **147**, 167–174.

2 I. El Saliby, L. Erdei, J. H. Kim and H. K. Shon, *Water Res.*, 2013, **47**, 4115–4125.

3 R. G. Li, H. X. Han, F. X. Zhang, D. G. Wang and C. Li, *Energy Environ. Sci.*, 2014, **7**, 1369–1376.

4 S. Jia, J. Li, G. Sui, L. Du, Y. Zhang, Y. Zhuang and B. Li, *RSC Adv.*, 2019, **9**, 31177–31185.

5 R. M. Ali, M. R. Elkatory and H. A. Hamad, *Fuel*, 2020, **268**, 117297.

6 A. Y. Meng, J. Zhang, D. F. Xu, B. Cheng and J. G. Yu, *Appl. Catal., B*, 2016, **198**, 286–294.

7 X. Li, J. G. Yu and M. Jaroniec, *Chem. Soc. Rev.*, 2016, **45**, 2603–2636.

8 K. J. Ramos-Corella, M. Sotelo-Lerma, A. A. Gil-Salido, J. L. Rubio-Pino, O. Auciello and M. A. Quevedo-Lopez, *Materials and Technology*, 2019, **34**, 455–462.

9 C. P. Sajan, S. Wageh, A. A. Al-Ghamdi, J. G. Yu and S. W. Cao, *Nano Res.*, 2016, **9**, 3–27.

10 B. L. Yan, J. Zhou, X. Y. Liang, K. N. Song and X. T. Su, *Appl. Surf. Sci.*, 2017, **392**, 889–896.

11 H. Hamad, D. Bassyouni, E.-S. El-Ashtoukhy, N. Amin and M. Abd El-Latif, *Ecotoxicol. Environ. Saf.*, 2018, **148**, 501–512.

12 E. S. Z. El-Ashtoukhy, N. K. Amin, M. M. Abd El-Latif, D. G. Bassyouni and H. A. Hamad, *J. Cleaner Prod.*, 2017, **167**, 432–446.

13 D. Bassyouni, M. Mohamed, E.-S. El-Ashtoukhy, M. A. El-Latif, A. Zaatout and H. Hamad, *Microchem. J.*, 2019, **149**, 103998.

14 H. Shokry, M. Elkady and H. Hamad, *J. Mater. Res. Technol.*, 2019, **8**, 4477–4488.

15 T. Shalaby, H. Hamad, E. Ibrahim, O. Mahmoud and A. Al-Oufy, *Ecotoxicol. Environ. Saf.*, 2018, **162**, 354–364.

16 X. H. Jia, R. R. Dai, D. D. Lian, S. Han, X. Y. Wu and H. J. Song, *Appl. Surf. Sci.*, 2017, **392**, 268–276.

17 Y. C. Yao, X. R. Dai, X. Y. Hu, S. Z. Huang and Z. Jin, *Appl. Surf. Sci.*, 2016, **387**, 469–476.

18 M. Fathy, H. Hamad and A. E. H. Kashyout, *RSC Adv.*, 2016, **6**, 7310–7316.

19 H. Hamad, E. Bailón-García, S. Morales-Torres, F. Carrasco-Marín, A. F. Pérez-Cadenas and F. J. Maldonado-Hódar, *J. Environ. Chem. Eng.*, 2018, **6**, 5032–5041.

20 A. A. Lopera, E. A. Chavarriaga, H. A. Estupinan, I. C. Valencia, C. Paucar and C. P. Garcia, *J. Phys. D: Appl. Phys.*, 2016, **49**(20), 205501.

21 T. Z. Xu, H. Zheng, P. Y. Zhang, W. Lin and Y. Sekiguchi, *J. Mater. Chem. A*, 2015, **3**, 19115–19122.

22 H. Hamad, J. Castelo-Quibén, S. Morales-Torres, F. Carrasco-Marín, A. F. Pérez-Cadenas and F. J. Maldonado-Hódar, *Materials*, 2018, **11**, 1766.

23 W. Y. Yan, Q. Zhou, X. Chen, X. J. Huang and Y. C. Wu, *Sens. Actuators, B*, 2016, **230**, 761–772.

24 H. Hamad, E. Bailón-García, F. J. Maldonado-Hódar, A. F. Pérez-Cadenas, F. Carrasco-Marín and S. Morales-Torres, *Appl. Catal., B*, 2019, **241**, 385–392.

25 D. Li, F. Chen, D. L. Jiang, W. D. Shi and W. J. Zheng, *Appl. Surf. Sci.*, 2016, **390**, 689–695.

26 L. Wang, L. Zang, J. C. Zhao and C. Y. Wang, *Chem. Commun.*, 2012, **48**, 11736–11738.

27 H. G. Yang, C. H. Sun, S. Z. Qiao, J. Zou, G. Liu, S. C. Smith, H. M. Cheng and G. Q. Lu, *Nature*, 2008, **453**, 638–641.

28 H. G. Yang, G. Liu, S. Z. Qiao, C. H. Sun, Y. G. Jin, S. C. Smith, J. Zou, H. M. Cheng and G. Q. Lu, *J. Am. Chem. Soc.*, 2009, **131**, 4078–4083.

29 X. G. Han, Q. Kuang, M. S. Jin, Z. X. Xie and L. S. Zheng, *J. Am. Chem. Soc.*, 2009, **131**(9), 3152–3154.

30 K. L. Lv, Q. J. Xiang and J. G. Yu, *Appl. Catal., B*, 2011, **104**, 275–281.

31 X. Bai, L. L. Lv, X. Y. Zhang and Z. L. Hua, *J. Colloid Interface Sci.*, 2016, **467**, 1–9.

32 J. S. Chen, Y. L. Tan, C. M. Li, Y. L. Cheah, D. Y. Luan, S. Madhavi, F. Y. C. Boey, L. A. Archer and X. W. Lou, *J. Am. Chem. Soc.*, 2010, **132**, 6124–6130.

33 H. M. Zhang, Y. H. Han, X. L. Liu, P. R. Liu, H. Yu, S. Q. Zhang, X. D. Yao and H. J. Zhao, *Chem. Commun.*, 2010, **46**, 8395–8397.

34 Y. L. Liu, L. L. Wang, W. Jin, C. Zhang, M. Zhou and W. Chen, *J. Alloys Compd.*, 2017, **690**, 604–611.

35 W. G. Yang, J. M. Li, Y. L. Wang, F. Zhu, W. M. Shi, F. R. Wan and D. S. Xu, *Chem. Commun.*, 2011, **47**, 1809–1811.

36 M. Liu, L. Y. Piao, W. M. Lu, S. T. Ju, L. Zhao, C. L. Zhou, H. L. Li and W. J. Wang, *Nanoscale*, 2010, **2**, 1115–1117.

37 W. X. Huang, *Acc. Chem. Res.*, 2016, **49**, 520–527.

38 L. Zhang, D. C. Shi, B. C. Liu, G. Zhang, Q. Wang and J. Zhang, *Crystengcomm*, 2016, **18**, 6444–6452.

39 B. Han, Q. Dong, J. Chen, W. Feng, S. L. Liu and H. L. Wang, *J. Adv. Oxid. Technol.*, 2015, **18**, 98–104.

40 S. Yurdakal, B. S. Tek, C. Degirmenci and G. Palmisano, *Catal. Today*, 2017, **281**, 53–59.

41 D. X. M. Vargas, J. R. De la Rosa, C. J. Lucio-Ortiz, A. Hernandez-Ramirez, G. A. Flores-Escamilla and C. D. Garcia, *Appl. Catal., B*, 2015, **179**, 249–261.

42 G. Sui, J. Li, L. Du, Y. Zhuang, Y. Zhang, Y. Zou and B. Li, *J. Alloys Compd.*, 2020, **823**, 153851.

43 X. Q. Li and W. X. Zhang, *J. Phys. Chem. C*, 2007, **111**, 6939–6946.

44 J. G. Darab, A. B. Amonette, D. S. D. Burke, R. D. Orr, S. M. Ponder, B. Schrick, T. E. Mallouk, W. W. Lukens, D. L. Caulder and D. K. Shuh, *Chem. Mater.*, 2007, **19**, 5703–5713.

45 Z. Q. Fang, J. H. Chen, X. H. Qiu, X. Q. Qiu, W. Cheng and L. C. Zhu, *Desalination*, 2011, **268**, 60–67.

46 S. N. Xu and Z. Q. Hu, *Water Environ. Res.*, 2015, **87**, 483–490.

47 X. Y. Wang, P. Wang, J. Ma, H. L. Liu and P. Ning, *Appl. Surf. Sci.*, 2015, **345**, 57–66.

48 J. Zhang, G. L. Zhang, K. Zheng, D. Q. Cai and Z. Y. Wu, *J. Nanosci. Nanotechnol.*, 2015, **15**, 6103–6107.

49 Z. M. Yang, X. H. Qiu, Z. Q. Fang and T. Pokeung, *Water Sci. Technol.*, 2015, **71**, 1800–1805.

50 J. Soukupova, R. Zboril, I. Medrik, J. Filip, K. Safarova, R. Ledl, M. Mashlan, J. Nosek and M. Cernik, *Chem. Eng. J.*, 2015, **262**, 813–822.

51 X. N. Fei, L. Y. Cao, L. F. Zhou, Y. C. Gu and X. Y. Wang, *Water Sci. Technol.*, 2012, **66**, 2539–2545.

52 W. P. Hsieh, J. R. Pan, C. P. Huang, Y. C. Su and Y. J. Juang, *Sci. Total Environ.*, 2010, **408**, 672–679.

53 Y. Dong, X. Fei, L. Cao, R. Wu and Y. Jiang, *RSC Adv.*, 2015, **5**, 92677–92684.

54 C. P. Huang, W. P. Hsieh, J. R. S. Pan and S. M. Chang, *Sep. Purif. Technol.*, 2007, **58**, 152–158.

55 L. F. Liu, F. Chen, F. L. Yang, Y. S. Chen and J. Crittenden, *Chem. Eng. J.*, 2012, **181**, 189–195.

56 Y. Dong, X. Fei and Y. Zhou, *Appl. Surf. Sci.*, 2017, **403**, 662–669.

57 Y. Dong, X. Fei, Z. Liu, Y. Zhou and L. Cao, *Appl. Surf. Sci.*, 2017, **394**, 386–393.

58 I. Levchuk, M. Sillanpaa, C. Guillard, D. Gregori, D. Chateau and S. Parola, *Appl. Surf. Sci.*, 2016, **383**, 367–374.

59 M. Rastgar, A. R. Zolfaghari, H. R. Mortaheb, H. Sayahi and H. R. Naderi, *J. Adv. Oxid. Technol.*, 2013, **16**, 292–297.

60 X. Sun, T. Kurokawa, M. Suzuki, M. Takagi and Y. Kawase, *J. Environ. Sci. Health, Part A: Toxic/Hazard. Subst. Environ. Eng.*, 2015, **50**, 1057–1071.

61 Y. J. Wang, Y. M. He, T. T. Li, J. Cai, M. F. Luo and L. H. Zhao, *Chem. Eng. J.*, 2012, **189**, 473–481.

62 H. A. Hamad, W. A. Sadik, M. M. Abd El-latif, A. B. Kashyout and M. Y. Feteha, *J. Environ. Sci.*, 2016, **43**, 26–39.

63 S. Bae, J. Jung and W. Lee, *Chem. Eng. J.*, 2013, **232**, 327–337.

64 M. Elkady, H. Shokry, A. El-Sharkawy, G. El-Subruiti and H. Hamad, *J. Mol. Liq.*, 2019, **294**, 111628.

65 A. T. Kuvarega, R. W. M. Krause and B. B. Mamba, *Appl. Surf. Sci.*, 2015, **329**, 127–136.

66 H. Liu, D. R. Li, X. L. Yang and H. F. Li, *Materials and Technology*, 2019, **34**, 192–203.

67 S. P. Kim and H. C. Choi, *Bull. Korean Chem. Soc.*, 2015, **36**, 258–264.